Available online at www.sciencedirect.com
SCIENCE DIRECT®
International Journal of Heat and Fluid Flow 25 (2004) 795–808
International Journal of HEAT AND FLUID FLOW
www.elsevier.com/locate/ijhff

The negatively buoyant wall-jet: LES results

Y. Addad [a], S. Benhamadouche [a,b], D. Laurence [a,b,*]

[a] Thermofluids Division, MAME Department, UMIST, Manchester, M60 1QD, UK
[b] Electricité de France R&D, MFTT, 6 Quai Watier, Chatou F-78400, France

Received in revised form 16 May 2004; accepted 21 May 2004
Available online 10 July 2004

Abstract

The results of a Large-Eddy Simulations (LES) of a downward hot wall-jet injected against a cold upward channel flow are presented. Based on the experiment of He et al. (2002) [Int. J. Heat Fluid Flow 23 (2002) 487], this flow was suggested as an "application challenge" by the power generation industrial sector to the Qnet-CFD EU network. Indeed, numerical predictions vary significantly with the type of RANS model used, with only the most advanced models yielding reasonable agreement with the experiment as presented in a companion paper by Craft et al. [Int. J. Heat Fluid Flow 25 (2004) 809]. The present LES was attempted to hopefully confirm and complete the experimental data, which in some areas can be sparse. As resources limited the LES to 1/2 million nodes, an optimal LES mesh was defined from RANS derived scales. Then to reduce uncertainties, two independent codes are used to perform the simulations: the commercial code *Star-CD* and an industrial one, *Code_Saturne*. The statistical quantities compared with the experimental data show that both codes are able to return fairly satisfactory results for the isothermal and moderately buoyant cases. For the third and strongly buoyant case comparison was only qualitative.

1. Introduction

Large-eddy simulation (LES) is increasingly recognised as a major tool for studying details of turbulent engineering flows. The geometries already simulated using LES vary from relatively simple cases, as channel flows and backward facing steps (Koutmos and Mavridis, 1997), to more complex ones, for example concerning jets: gas turbine combustors (Mahesh et al., 2001), impinging jet flow (Gao and Voke, 1995), plane cross-flow (Jones and Wille, 1996) and T-junction (Benhamadouche et al., 2003). Since LES contains time-dependent information such as evolution of large eddies, instantaneous fluctuations, time traces of quantities, spectra and two-point correlations, it can give a much more realistic picture of certain aspects of turbulence than traditional methods of turbulence prediction.

Within the framework of a Thematic Network on Quality and Trust for the industrial applications of CFD (www.qnet-cfd.net), industrial partners have put forward "application challenges", i.e., test cases which are demanding from the turbulence modelling point of view and also relevant to core applications of specific industries. In the power generation thematic area, the application challenge of BNFL Magnox Generation corresponds to a downward hot wall jet injected against an upward cold channel flow. The problem is specifically relevant to the gas flow between the core and spherical steel pressure vessel of a Magnox reactor. The penetration depth of the jet, wall temperature fluctuations at the point of separation and subsequent mixing influence the temperature distribution within the pressure vessel. The problem is also relevant to other flows in nuclear power plants.

This configuration has been previously investigated experimentally by He et al. (2002) with the aim of producing data to support RANS modelling efforts. The present Large-Eddy Simulation study aims at expanding the data available, especially in the near wall region of the decelerating jet flow. It will also help answer a few questions that remained ambiguous while interpreting the experiment, such as the assumed two-dimensionality of the flow. Once a satisfactory flow database is obtained, this can then be exploited to develop and test

* Corresponding author. Tel.: +44-161-200-3704; fax: +44-161-200-3723.
E-mail address: dominique.laurence@UMIST.ac.uk (D. Laurence).

0142-727X/$ - see front matter © 2004 Elsevier Inc. All rights reserved.
doi:10.1016/j.ijheatfluidflow.2004.05.008

improved RANS turbulence models for buoyancy-influenced flows, with particular interest for the near-wall region.

At the beginning of the present investigation it was expected that the LES would agree with the rather sparse experimental data and provide further details, both approaches validating each other. However, in case no satisfactory agreements would be obtained, two completely different codes are used to enable some conclusive results as to whether this was due to the assumptions made concerning the experiment set-up, or insufficient the accuracy of the numerical method.

2. Numerical methods

2.1. Numerical solver

LES calculations are carried out using two different codes: One is the commercial code Star-CD and the second is *Code_Saturne* (Archambeau et al., 2004) developed at Electricité de France (EDF). Both have been tested on LES of complex flows with success (tube bundles (Benhamadouche and Laurence, 2003), gas turbine combustors (Benhamadouche et al., 2002), singularities in piping systems (Benhamadouche et al., 2003), blunt obstacle (Addad et al., 2003). Both codes use an unstructured, collocated finite-volume technique (Ferziger and Perić, 1999). *Code_Saturne* uses a second order centred scheme in space and time (Benhamadouche and Laurence, 2003; Benhamadouche, 2001). It is a global Crank–Nicholson scheme on both convection and diffusion. The non-linearity is treated by evaluating the mass flux with an Adams–Bashforth extrapolation. On the other hand, in STAR-CD convection contribution to the velocity increment is predicted by an upwind scheme and a centred spatial discretisation of the convection is introduced as a deferred correction (Ferziger and Perić, 1999). Crank–Nicholson is used for diffusion. The global scheme is thus second order in space for steady state and, formally, first order in time dependant flows, but the truncation error limited to the velocity increment (instead of the velocity itself) is small. This latter scheme is found to be very stable, which is a mandatory condition for a commercial code. In both codes and for the non-buoyant case presented hereafter, the thermal field is computed as a passive scalar for which the central discretisation is similar to that of momentum equations. A bounded scheme (MARS) is used for temperatures in Star-CD for the buoyant cases, as discussed later in Section 4.

2.2. Subgrid-scale models

The subgrid-scale model used in the simulations carried out with the commercial code is based on the standard Smagorinsky model in which the subgrid eddy-viscosity is derived from the local grid scale and strain rate:

$$\upsilon_s = \left(c_s f_\mu \Delta\right)^2 \left(2S_{ij}S_{ij}\right)^{1/2} \tag{1}$$

in which the local filter scale is defined by

$$\Delta = 2(\Delta_x \Delta_y \Delta_z)^{1/3}. \tag{2}$$

The subgrid eddy-viscosity must reduce to zero when approaching the solid wall. This is achieved by modifying the length scale with a Van Driest near-wall damping function f_μ. The Smagorinsky constant chosen is 0.059. Note that the original definitions are used above, whereas some recent publications tend to omit the factor 2 in (1) and (2), resulting in apparently higher values of the Smagorinsky constant. A full description of the constant calibration for the commercial code can be found in Addad et al. (2003), including homogeneous isotropic turbulence tests.

The dynamic version of the model is implemented in *Code_Saturne*, using the algorithm proposed by Germano with least squares. It automatically adjusts the constant at each point in space and at each time step, and avoids the use of Van Driest damping functions. Further details about the subgrid models implementation and validation in *Code_Saturne* are reported in Benhamadouche (Benhamadouche, 2001).

The thermal subgrid-scale model is based on a turbulent Prandtl number $Pr_t = 0.9$ or 0.4 (see Section 4).

2.3. Geometry and boundary conditions

The complete geometry, as shown in Fig. 1, is planar. The principal dimensions of the case are illustrated in Fig. 1, with the breadth of the computational domain being 0.3 m. Note that the same coordinate system notations as experimental paper of (He et al., 2002) is used herein, but differs from that in the Craft et al. companion paper. The Reynolds number of the simulation is $Re = 4000$ based on the bulk jet velocity and the jet width. The ratio of the background channel velocity to jet velocity is $V_{ch}/V_{jet} = 0.077$. The physical parameters are those of water at the temperature of 42 °C. The inlet fluid temperature in the wall jet and the upward channel are, respectively, 42 and 34 °C. The walls are assumed to be adiabatic.

The computation of the wall stress varies, depending on the size of the first cell at the wall, x^+. This boundary condition is the same as the natural no-slip condition in the sub layer, but changes into one form of the log-law model (or the power-law for *Code_Saturne*) beyond $x^+ = 11.81$. In one of the tests not presented here, the log-law was tested in *Code_Saturne* and it was observed to return the same results as the power law. This is not surprising as with the chosen near wall cell sizes both

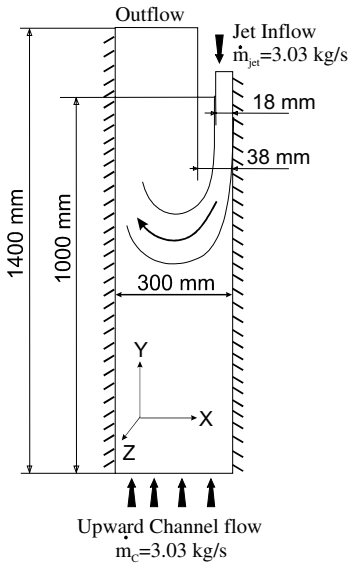

Fig. 1. The wall-jet flow geometry.

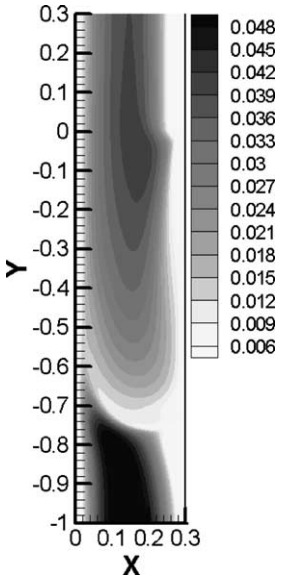

Fig. 2. The estimated integral length scale l_m from a low-Reynolds k-epsilon model.

approaches revert to the linear profile most of the time. At the inlet are prescribed fully developed channel-flow mean velocity profiles with superimposed random fluctuations, which are scaled using the corresponding turbulent kinetic energy profile. Periodicity is assumed in the homogeneous "z" direction. The outlet position is at $Y - Y_{\text{jet}} = 0.4$ m to avoid the effects of any adverse velocity from the outlet flow on the simulations results.

2.4. Grid generation and simulation feasibility

A proper LES must resolve all large turbulent scales in the flow, i.e., those containing most of the turbulent kinetic energy and Reynolds shear stress in each region of the flow. As a precaution, prior to the LES simulations, results obtained from a RANS model are used to estimate the integral length scale $l_m = C_\mu^{0.75} k^{1.5}/\varepsilon$. The grid spacing used in LES simulations should be some minimal ratio of this local length scale (Baggett et al., 1997).

Compilation of the k-epsilon model results gives an estimation of this length scale illustrated in Fig. 2. In the central region of the domain a maximum value of 2–5 cm is observed, while it is tending to 0 near the walls and in the free jet reversal zone. Accordingly, the mean value of the mesh step for the LES is about 1 cm in the core region and 10% of this value in the important near-wall and the wall-jet reversal regions. A second finer grid is generated using hanging nodes to further refine these two important regions. The resulting coarse and fine grids are presented in Fig. 3a and 3b, respectively. The refinement/coarsening is applied in all three directions to maintain a low cell aspect ratio as is desirable for LES.

The non-dimensional size of the near-wall cell at the wall-jet inlet is $\Delta x^+ = 9.4$ for the coarse grid (220,000 cells) and 4.7 for the fine mesh (601,000 cells), but then reduces as the jet decelerates. Fig. 4 shows the ratio Δ/l_m computed for the fine grid. This ratio is less or equal to unity, meaning that acceptable resolution is obtained in the core region of the domain and at the wall-jet frontier. However, the jet discharge region is undoubtedly under-resolved. In fact for a proper resolution in this region the grid size needs to be 4–5 times smaller but this was not possible, as this would have a large impact on the times-step and computational costs. Nevertheless, it can be argued that the turbulent scales in this part of the domain are very small compared to the turbulence within the region of interest, which is generated from the free shear flow and the jet reversal. In this free jet region

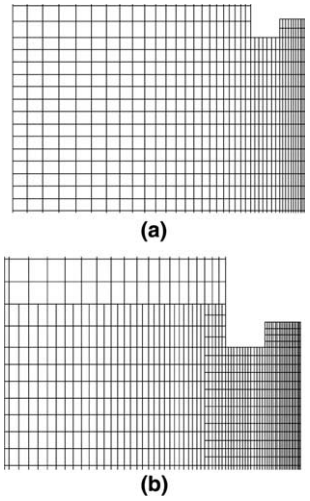

Fig. 3. (a) Coarse grid, (b) fine grid with hanging nodes.

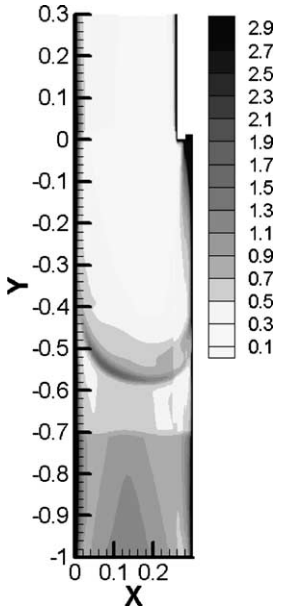

Fig. 4. Ratio between the grid filter Δ and the RANS integral length scale.

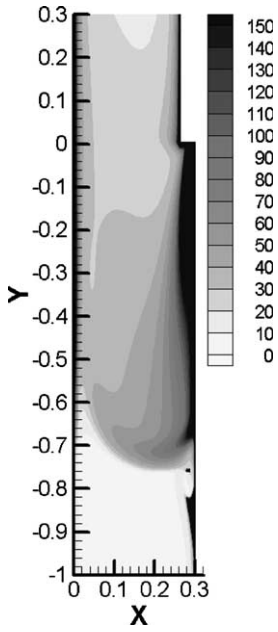

Fig. 5. Ratio between τ_{stat} and the RANS time scale k/ε.

the turbulent kinetic energy is a factor of 100 times larger than in the lower channel flow. I.e. the expectation (confirmed by later results) is that the region of the jet discharge, treated as a "Very Large Eddy-Simulation" and is playing a minor role in the flow development.

In the a priori study of industrial LES, the physical time τ_{stat} needed for the time-averaging statistics should also be estimated from the characteristic time scale k/ε, where k is the turbulent kinetic energy and ε is the turbulent dissipation rate. The ratio $\tau_{stat}/(k/\varepsilon)$ is presented in Fig. 5. A simulation time of the order of about $3V_{ch}/L_y$, where V_{ch} is the upward channel bulk velocity and L_y the streamwise domain dimension (i.e., three flow-through times), seems sufficient to obtain a quite satisfactory statistically converged solution in time (average of 50 large eddy turn-over times). A further averaging may also be performed in the homogeneous directions. In fact, the scalings from RANS results is fairly useful in determining the feasibility of undertaking an LES, but it should only be used as "qualitative" information. For instance the wall-jet penetration depth is largely over-predicted by RANS as it is discussed with details in Craft et al. (2004).

3. Non-buoyant simulations

3.1. Simulation description

Three non-buoyant jet simulations have been performed: STCL1 using the classical subgrid model in the commercial code and SAD1 and SAFIN using the dynamical form of the model with *Code_Saturne*. In each run, the first two passes through the domain were allowed for the turbulent field to settle into a physically realistic state before time-averaged statistics are gathered over three flow-through times. Information on the runs is summarised in Table 1. Computation where initially conducted on an outdated Origin 2000 then on a Linux PC. On an identical computer the two codes have similar speeds.

3.2. Analysis

Fig. 6 shows profiles of time-and-z-wise averaged stream-wise and horizontal velocities at successive vertical distances down from the splitter plate compared with the data of He et al. (2002). The comparison indicates that the LES computations are in quite satisfactory agreement with the experiment and with each other. The

Table 1
The LES runs performed for the upward channel opposed wall-jet

Run	Grid	Code	Model
STCL1	Coarse 356 000	Star-CD	Smagorinsky
SAD1	Coarse 356 000	*Code_Saturne*	Dynamic
SAFIN	610 000 unstructured	*Code_Saturne*	Dynamic

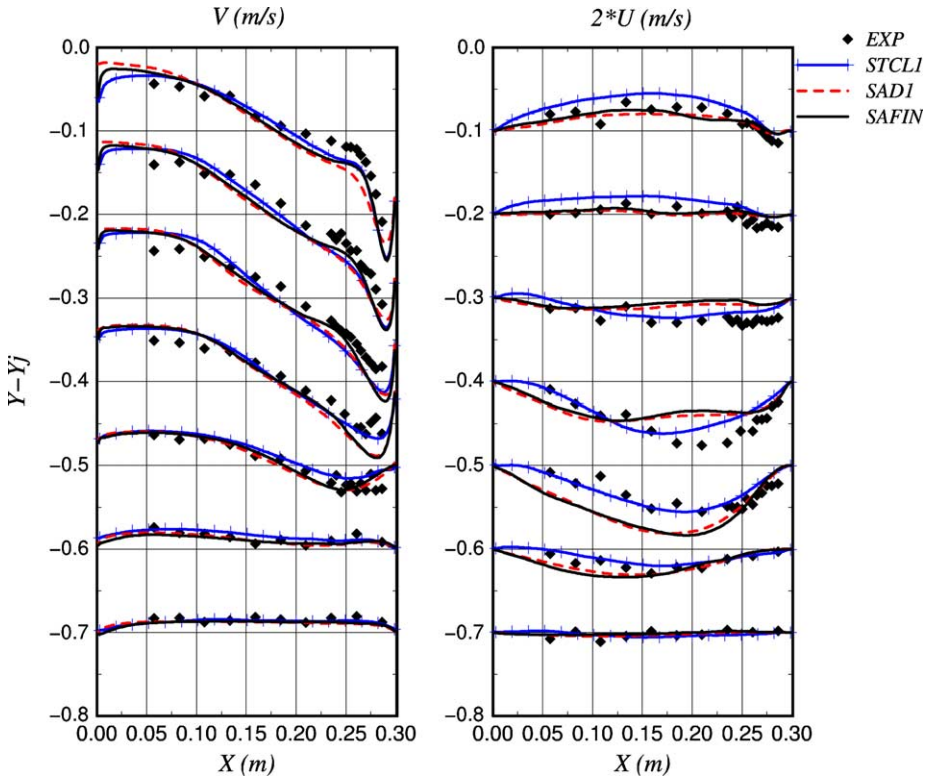

Fig. 6. Time and space averaged vertical and horizontal velocities. Each profile at an altitude $y = y_s$ is shifted by the value y_s, ($f(x) = V(x, y_s) + y_s$ and $f(x) = 2U(x, y_s) + y_s$ are plotted left and right, respectively). Note that the same coordinate system notations as experimental paper of He et al. (2002) is used herein.

wall-jet penetration and reversal are correctly predicted in all the runs. The profiles of the vertical and horizontal rms fluctuations also compare well with the experimental results in Fig. 7. At all but one location, the differences between the three LES results seem to be within the experimental noise. The main differences are observed on the profile at $Y - Y_j = -0.4$, the *Code_Saturne* results indicating a somewhat delayed flow reversal.

Some tests performed with *Code_Saturne* and the classical Smagorinsky model, not shown here, returned unusually large fluctuations in the wall-jet discharge region. This may be expected when using a fully centred discretisation in an under-resolved region, as is case for the jet outlet, and could be expected from the a-priori analysis. This is suggesting that the algorithm used in the commercial code, with an upwind predictor step, is acting favourably in the present case. A higher value of the Smagorinsky constant in *Code_Saturne* removed perturbations, but switching to a dynamic procedure also resolved instabilities in the under-resolved region and thus only this approach was pursued until full statistical convergence, even for the coarse mesh. It is interesting to notice the smooth rms profiles of the SAFIN run in the local refinements regions with hanging nodes. This is in contrast with reservations one might have for using hanging nodes with LES, due to the discontinuity of the eddy-viscosity and interpolations at this non-conforming interface, not to mention commutation errors between derivatives and filtering. However, no perturbations are observed here. This was also the case in a previous study with again extensive use of hanging nodes (Addad et al., 2003).

Fig. 8 shows the friction coefficient profiles along the wall-jet obtained with the different LES runs. The results obtained with RANS models using the analytical wall functions presented in the companion paper by Craft et al. (2004) are also added. Experimental data are not available in this region. The three LES results are in fair agreement with each other, the *Code_Saturne* runs with coarse and fine mesh are surprisingly not very different. The more elaborate second moment RANS model (TCL) with advanced wall functions, is clearly much closer to the LES results. It should be mentioned that the LES results became available only after the RANS runs had been obtained, so no adjustment of the wall functions was made by the authors of the companion paper to fit the present data.

LES and advanced RANS results exhibit a similar negative peak below the separation. This acceleration of the upward flow may be due to entrainment by the separating jet. It is also re-assuring that the LES and RANS results near the jet exit are in reasonable agreement although it would have been preferable to impose

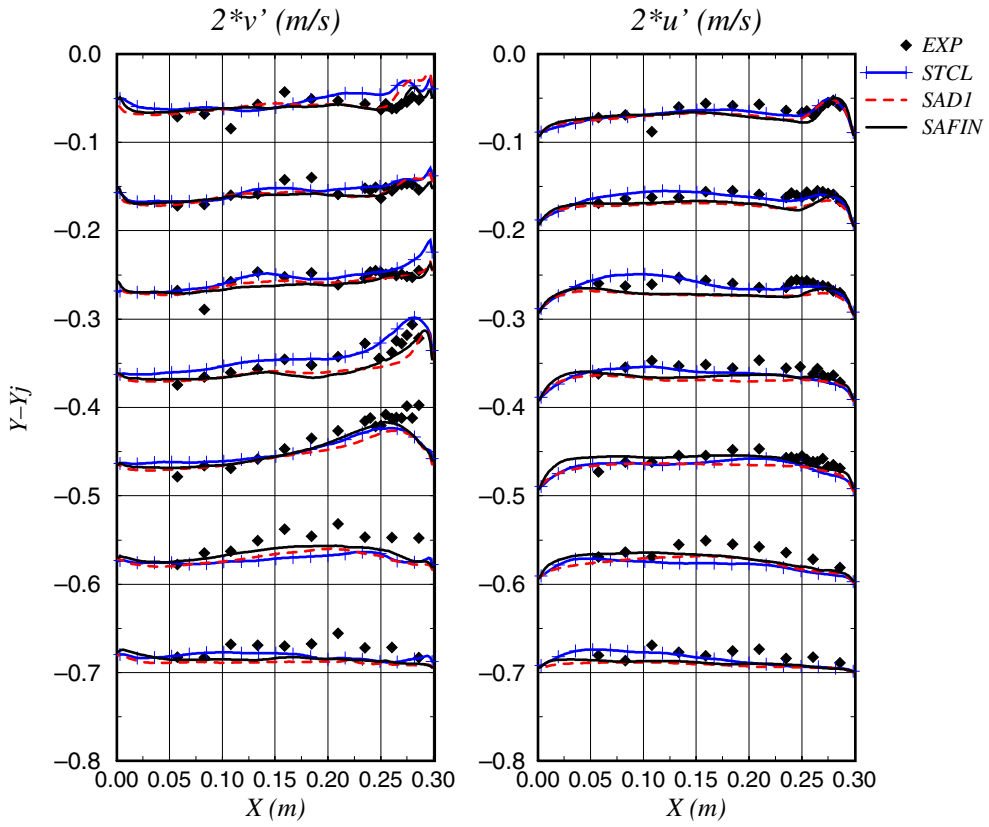

Fig. 7. Time and space averaged vertical and horizontal rms fluctuations. Same remarks as Fig. 6.

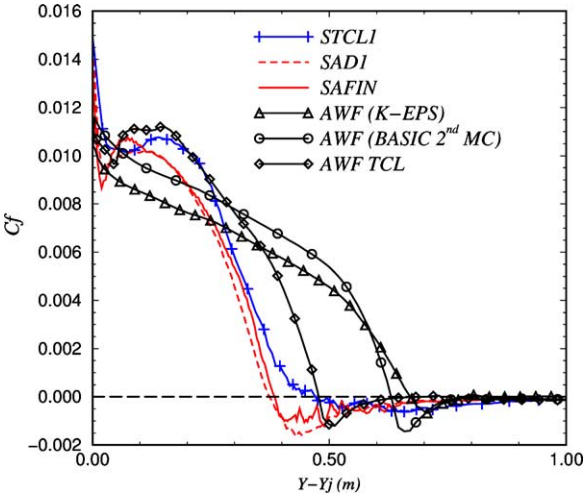

Fig. 8. The friction coefficient. The results of the RANS are obtained from Craft et al.

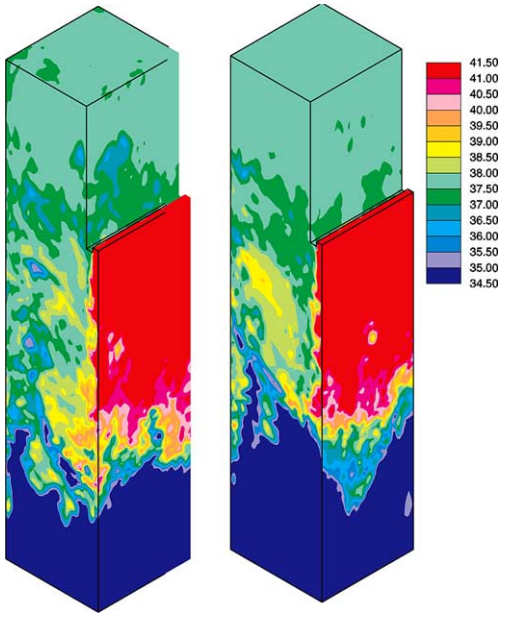

Fig. 9. The temperature field at times t and $t + \tau_{stat}$.

inlet conditions for the LES corresponding to a precursor channel flow simulation.

Fig. 9 shows the instantaneous scalar field after the establishment of the flow, these are "snap-shots", from an animation of temperature variations in the wall jet region. The separation is seen to be very three-dimensional and unsteady. Fig. 10 illustrates the temperature as a function of time at three points at the altitude

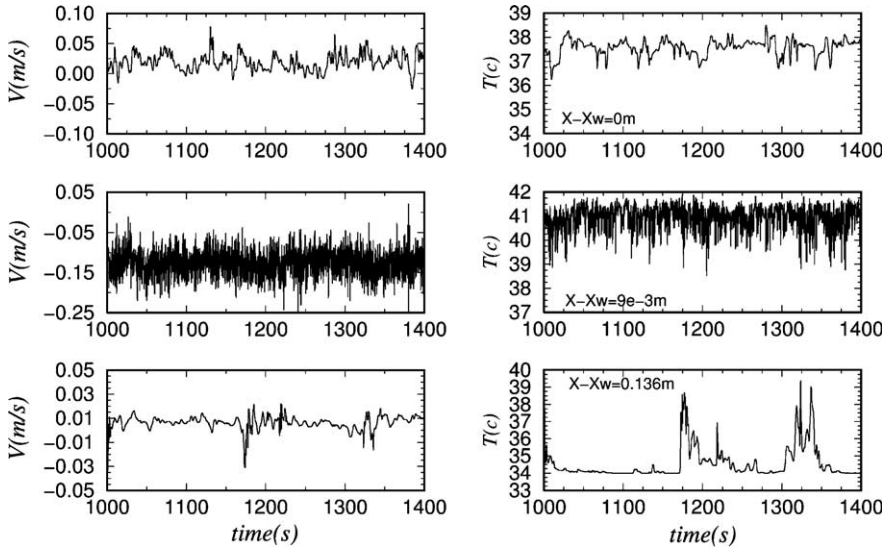

Fig. 10. Temperature variation in time (right) and vertical velocity variation (left) for three horizontal points at $Y - Y_j = -0.65$ m.

$Y - Y_{\text{jet}} = -0.65$ m from the wall-jet discharge, i.e., just below the separated jet. The clearly visible intermittency at the most central position is a result of large fluctuations in the position of the jet separation, as is seen from animations and Fig. 9.

4. Buoyant cases

In the previous simulations, temperature was included as a passive scalar and compared to the isothermal experiment. In the following cases, gravity is activated in the computations. In the first case, BUO1, the ratio of the background channel velocity to jet velocity is again $V_{\text{ch}}/V_{\text{jet}} = 0.077$ while in the case BUO2 the lower channel velocity is increased such that $V_{\text{ch}}/V_{\text{jet}} = 0.15$. For these cases only the Star-CD code was used. Also the MARS convective scheme was used for the temperature discretisation. This scheme specific to Star-CD is based on a TVD method for computation of gradients and some moderate blending of upwinding in the convection scheme. The intermediate tests carried out using the central and MARS schemes showed that the latter returns bounded temperature values, thus no clipping was needed to maintain realistic physical values of temperature within the domain. On the other hand, the MARS scheme is known to be more dissipative, hence the reason for choosing a higher value of 0.9 for the turbulent Prandtl number initially (for velocities central differencing is always used). A smaller Prandtl number value of 0.4, more conventional in LES, was also tested for a fully converged run and those results overlapped with the previous ones. In this test case, with no wall heat transfer, the SGS Prandtl number value seems to have a quite insignificant influence on the results.

4.1. Simulation set-up

The same procedure as explained in Section 3 was again adopted to generate the grid for the buoyant cases. The computational investigations of these cases with RANS models carried out by Craft et al. (2004) indicated a large sensitivity of the position of the jet reversal region to the top outlet position. This could be due the difficulty of imposing outlet conditions in a section still presenting density variations with buoyancy. The computations require a longer channel above the jet for the temperature profiles to reach uniformity (temperature profiles at the outlet of the shorter experimental rig were not measured). Thus, a longer computational domain than the experiment, and similar to the one used in RANS calculations, was chosen. The exit region of the computational domain was positioned at 2.4 m from the jet discharge as shown in Fig. 11. Four levels of grid refinements with hanging nodes as shown in Fig. 11 were used to enhance the resolution near the wall jet. The near-wall cell width is reduced to one viscous unit at the exit because in the buoyant cases the jet separates earlier, before deceleration and shear layer thickening. Hanging nodes are introduced in the three directions to limit the aspect ratio. The nodes are clustered on the right hand side wall at the detriment of the core and opposite wall regions because this is where the RANS simulations predicted the jet to be confined. The resulting mesh size has 700,000 cells. The total CPU time is nearly double the one for the isothermal case due to the elongated domain.

4.2. Analysis

Fig. 12 shows the averaged vertical velocity field for both velocity ratios. For case BUO1, in a satisfactory

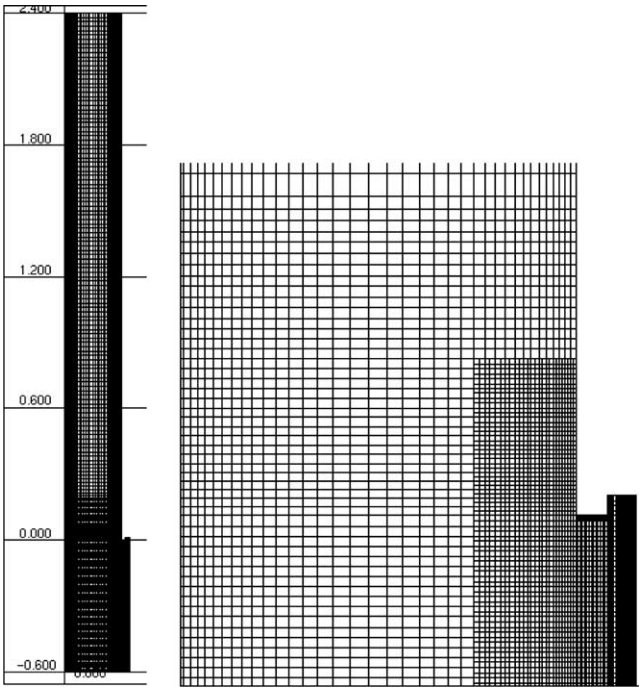

Fig. 11. Mesh used for the buoyant cases computations. Left, extended domain, above, zoom in the region around the jet discharge.

agreement with the experiment, the LES computations predict a reduction of the wall-jet penetration to 30% of the isothermal case ($V_{ch}/V_{jet} = 0.0077$) due to buoyancy effects. The penetration is further reduced when a higher upward channel velocity is applied $V_{ch}/V_{jet} = 0.15$ (BUO2) where the jet separates very soon after the exit. The qualitative agreement concerning the location of the overall jet centreline is seen from isovalue plots (Figs. 13 and 14), but the experimental data is now sparse and does not extend all the way to the walls. The penetration depth of the jet seems reasonably predicted, but in the horizontal direction the experiments indicate that the jet reverses before reaching the opposite wall, which is not the case in the LES. On Fig. 12, case BUO2, the LES shows that in the upper part the jet switches back to the right wall.

The horizontal fluctuations from both buoyant runs are presented in Fig. 13. A fairly satisfactory agreement of turbulence levels between the experimental data and the computations is observed. However, the upper part of the LES results seem to suffer from somewhat lower fluctuations values, which may be attributed to the low grid resolution away from the right wall (see Fig. 11). The experiment and LES show two distinctive peaks after reversal in BUO1. Animations of this flow show periodical flapping of the flow with hot plumes attaching the left and right walls alternatively as suggested by Fig. 17.

In contrast with the isothermal case where the turbulence is generated by the free shear flow around the jet, buoyancy forces now significantly complicate the interpretation. It is difficult to relate the present flow to natural convection or stratified flows to discuss stabilising/destabilising effects. However, animations tend to suggest that destabilising gravity effects dominate in BUO1 case. The wall jet separation line on the right wall shows a distinctive gravity-wave like behaviour along the homogeneous direction, with a wave-length corresponding to the width of the computational domain, which thus may be insufficient (Fig. 18). This low frequency oscillation could also explain the difficulties found in converging the 2D and steady RANS calculations using second moment models as discussed in the companion paper. For the higher counter-flow rate, BUO2, the jet separates from the wall very early along a

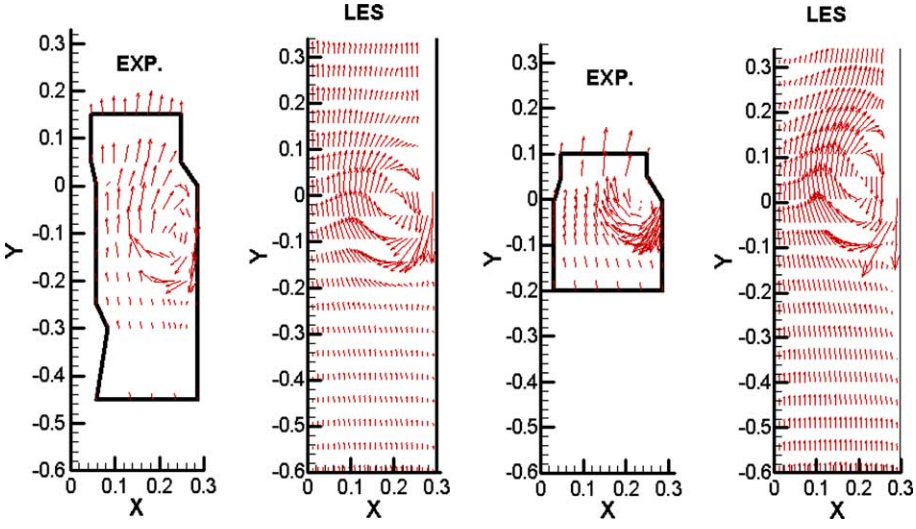

Fig. 12. Velocity vector plot; LES in comparison with the experiment. Left, low channel/jet velocity ratio 0.0077 (BUO1), right high velocity ratio 0.15 (BUO2).

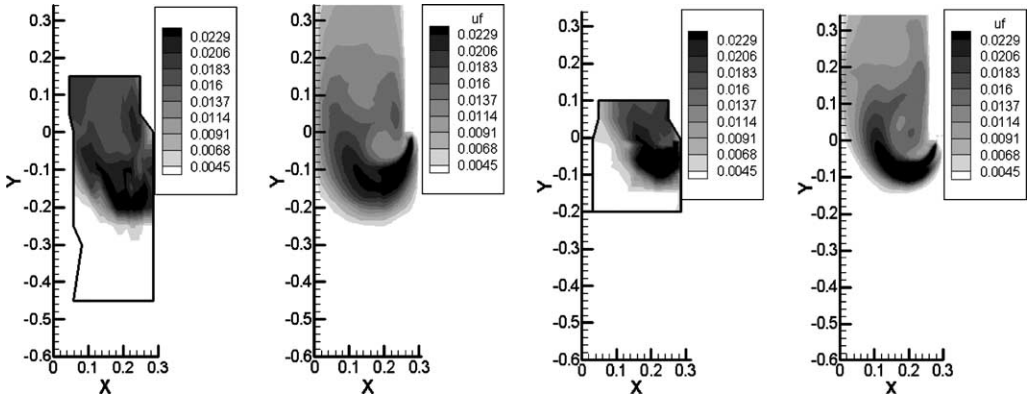

Fig. 13. rms horizontal velocity fluctuations. Left-BUO1 and right-BUO2, as Fig. 12.

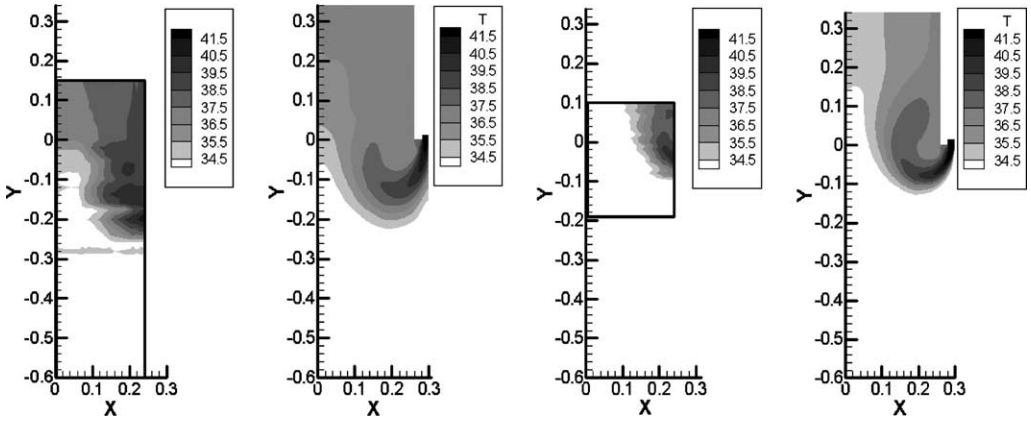

Fig. 14. Mean temperature distribution. Left-BUO1 and right-BUO2 as Fig. 12.

sharp horizontal and steady line. The absence of large-scale unsteadiness makes this case more accessible to RANS models.

The averaged temperature field is presented in Fig. 14 and is consistent with the previous observations. The Y positions of jet reversal are well predicted, but the penetrations of the jet in the X direction are overestimated by the LES (however, experimental data points are quite sparse). The LES and RANS predictions presented in the companion paper of Craft et al. (with a hot bulb clinging to the jet exit) are in opposition in this respect, while the experimental pattern is between both predictions.

Figs. 15 and 16 show profiles of time-and-z-wise averaged stream-wise and horizontal velocities as well as rms profiles at successive vertical distances down from the splitter plate for both buoyant cases, compared with the data of He et al. (2002). For the lower aspect ratio case, only a qualitative agreement with the experiment is obtained as stated previously. The profiles show that detachment of the flow occurs too early, and this is most obvious from the horizontal component profile at $Y = -0.2$. The profiles at $Y = 0$ show that after reversal the jet centreline (velocity maximum) is shifted too far away from the right wall, in the LES. On the contrary, the k-epsilon results show a very sharp reversal of the jet and the separation from the wall occurs much lower than in the experiment. The fluctuation levels are fairly well predicted by the LES. The very low levels of fluctuations on the left hand side of the RANS simulation are explained by the fact that the jet is predicted confined to the right half of the channel (and unfortunately the mesh generation relied too heavily on these erroneous predictions). The LES results are superior to the k-epsilon ones, but not accurate enough to serve as validation for the advanced RANS models.

The results obtained in case BUO2 are found to be in a better agreement with the experiment (Fig. 16). The jet separation is remarkably well captured. The level of turbulence is also in a satisfactory agreement with experiment. The main difference between the present LES and the experimental data remains in the central region, where again the jet axis after reversal is shifted towards the left wall. This supports the

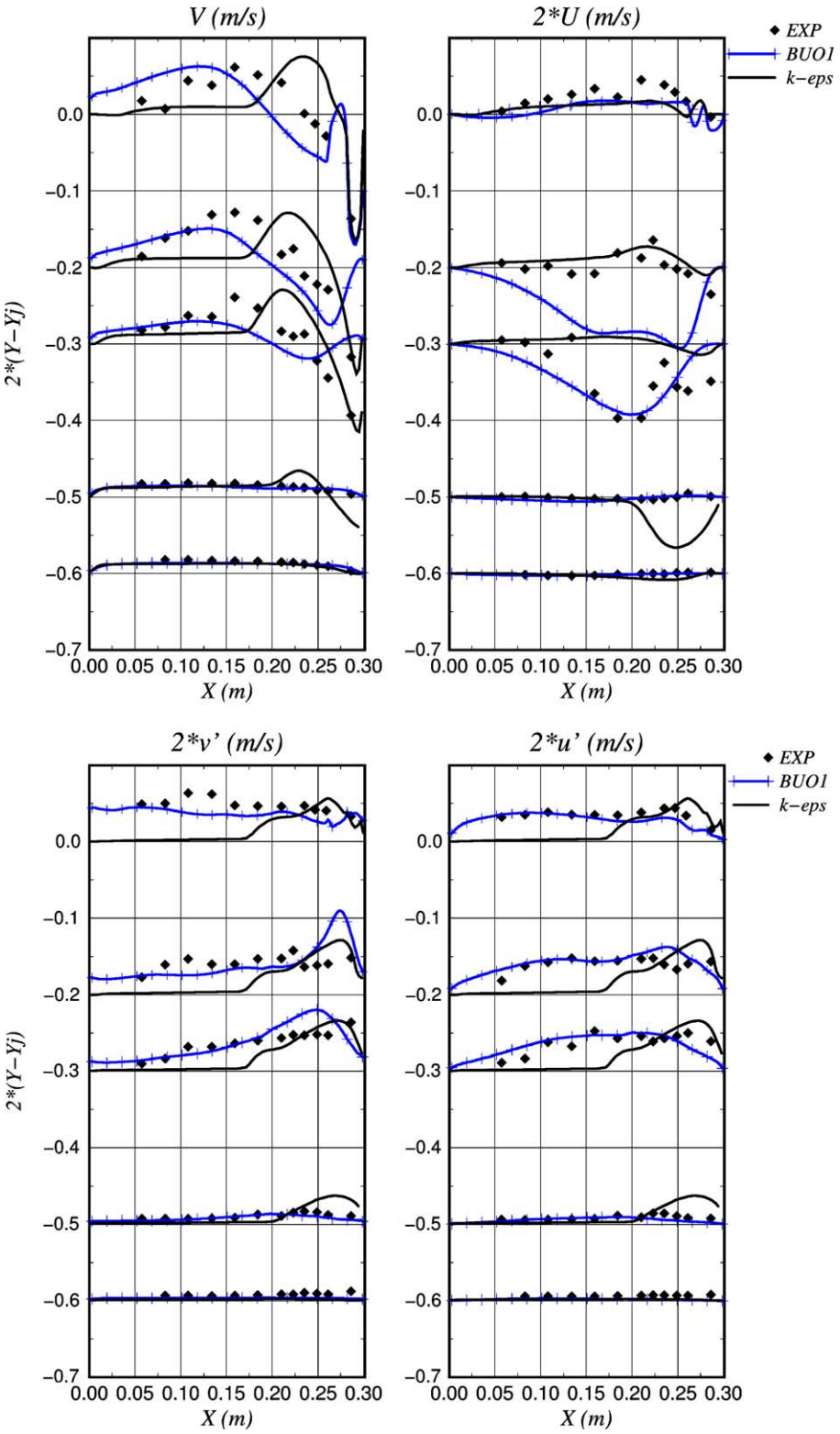

Fig. 15. Mean and rms velocity profiles for the low aspect velocity ratio case (BUO1). Each profile at an altitude $y = y_s$ is shifted by the amount $2y_s$.

suggestion that the different outlet configuration between the experiment and simulations may be the actual cause of this discrepancy for this case as well as the previous one. However, as far as the jet near wall region is concerned, the results from BUO2 are in good agreement with the experiment and may be used with confidence for RANS models validation.

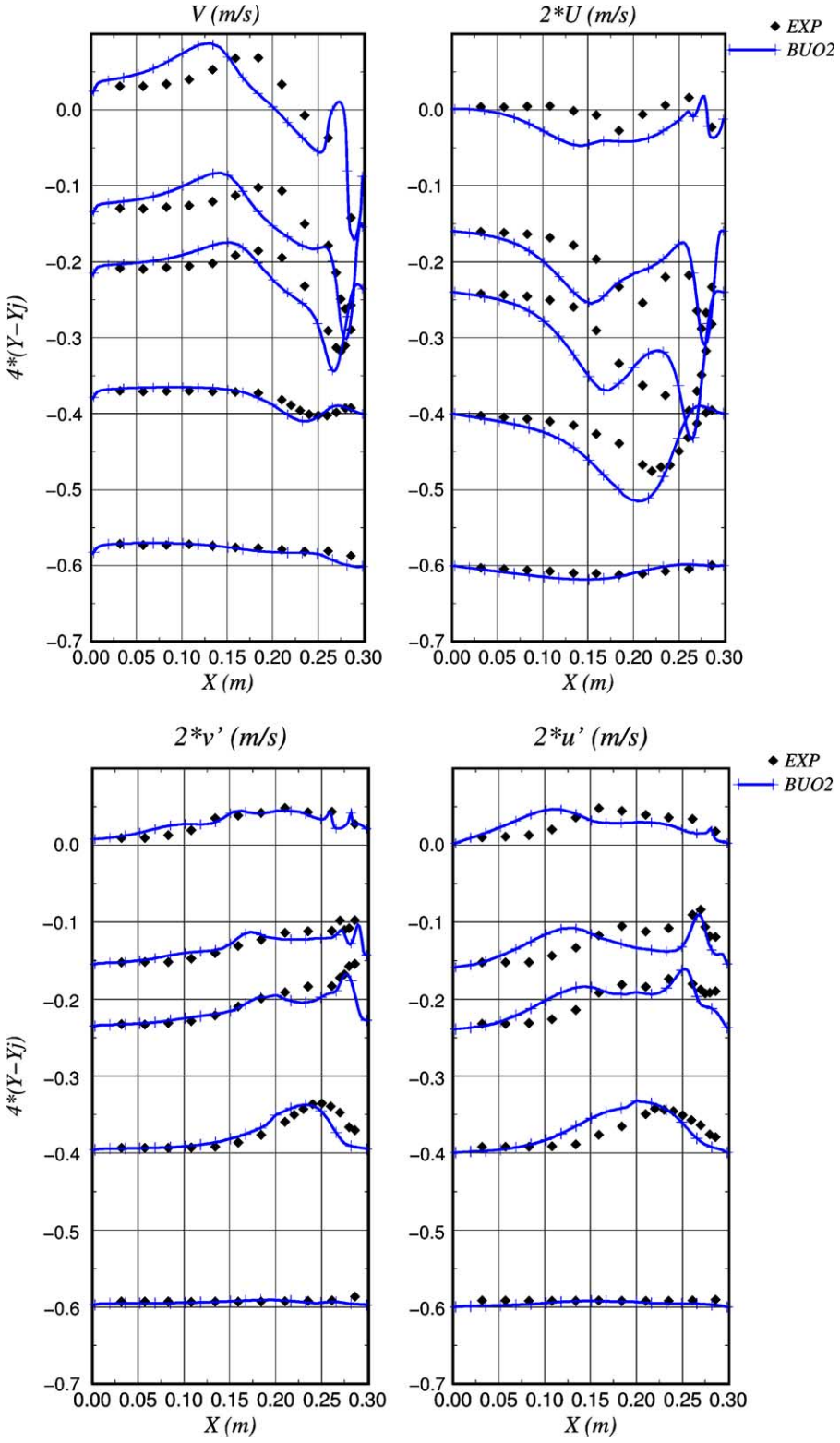

Fig. 16. Mean and rms velocity profiles for the high aspect velocity ratio case (BUO2).

Fig. 17 presents the instantaneous temperature field distribution of both buoyant cases at two different physical times. In BUO1 the hot–cold interface along the wall at the jet separation location is observed (in animations) to have a clear gravity-wave like behaviour, and further downstream, the maximal values oscillating

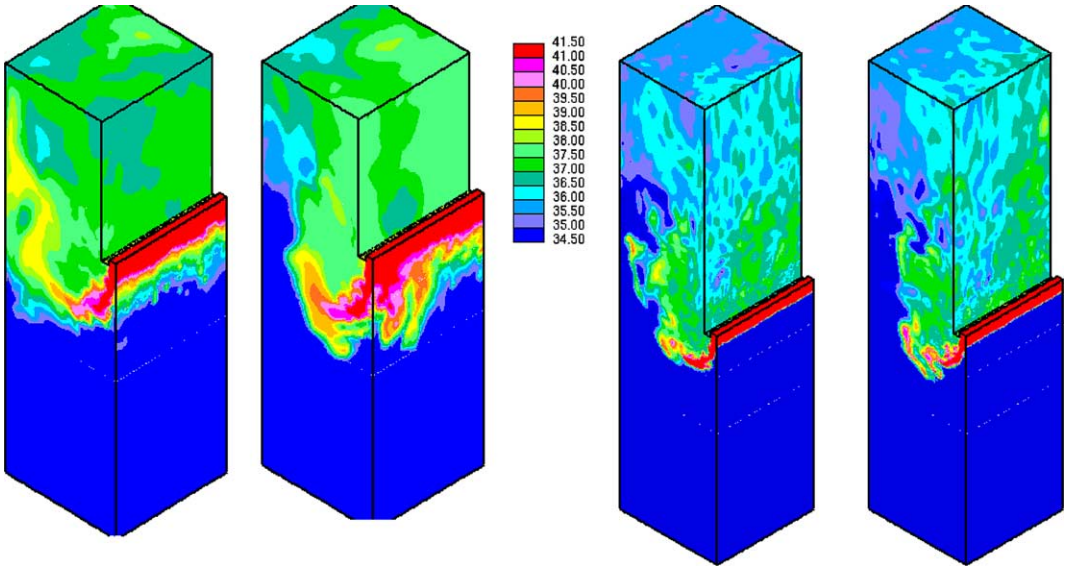

Fig. 17. Instantaneous temperature field at time t and $t + \tau_{stat}$. Low channel velocity—BUO1 on left, high channel velocity—BUO2 on the right.

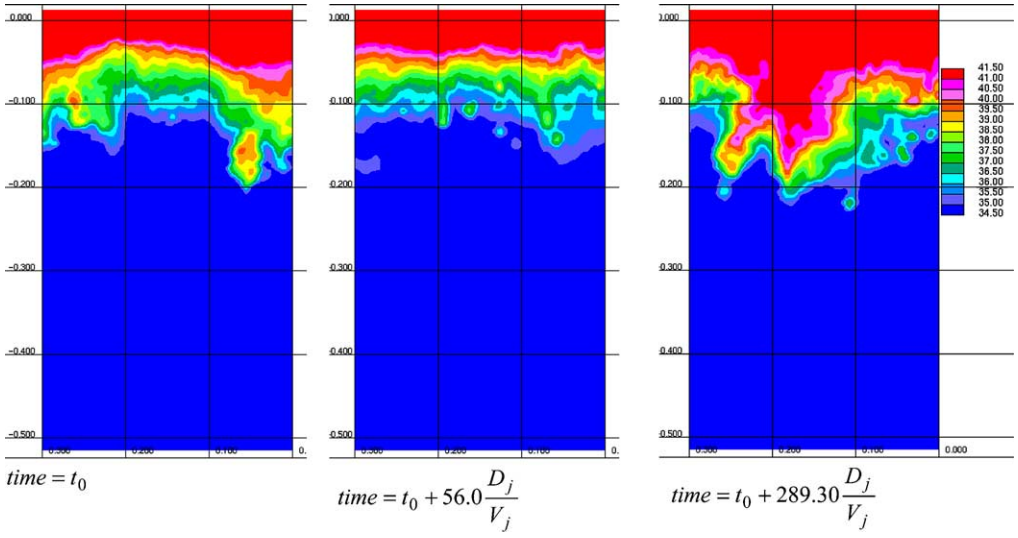

Fig. 18. Temperature at the wall for case BUO1 at different physical times.

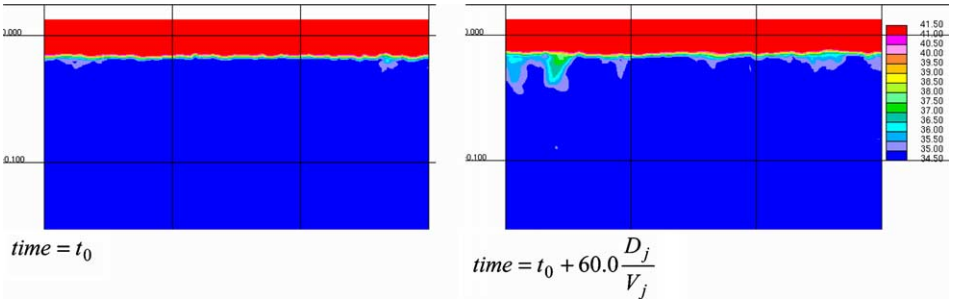

Fig. 19. Temperature at the wall for case BUO2 at different physical times.

between the channel centre and the opposite wall. In contrast, in the BUO2 case the hot fluid is more restricted to the right hand side. As shown in Figs. 18 and 19, the temperature gradient at the wall is sharper. In both cases, the three-dimensional behaviour of the jet separation along the wall is much less pronounced in comparison to the non-buoyant case (Fig. 9).

5. Conclusions

The present study of the downward wall-jet flow gives a good example of fairly complex and industry related flows that may be tackled by LES. Scalings obtained from a rough RANS simulation enabled a feasibility study and meshing guidelines prior to the LES. The LES predictions of mean quantities and low-order statistics, especially for the isothermal case, are in sufficient agreement with the experiments even with a fairly coarse grid. Hanging nodes are found very useful in adapting the local refinement to the large eddy scales, and only where it is needed, this without any noticeable adverse effects although the filter size discontinuity may raise theoretical issues. The dynamic model was found to resolve numerical problems in under-resolved regions where purely central differencing is used, but surprisingly the standard Smagorinsky model combined with slight upwinding (limited to the predictor step) in the commercial code faired just as well.

Near wall data and wall shear stress distributions can provide important information for near wall modelling proposes. Added to the experiment, the LES confirm the challenging nature of the test case, and support the companion RANS paper, which observes that standard models are inadequate while only the most advanced RANS models are able to predict the early jet separation from the wall. LES results obtained for the buoyant case with the low counterflow velocity, BUO1, show a more "qualitative" agreement with the experimental data. While the RANS predictions underestimate the capacity for the jet to cross over to the opposite side, the LES overestimates this feature (the experiments being in between). LES results for the second buoyant case, BUO2, with higher counterflow and hence lower buoyancy effects, are in better agreement with the experiment for both mean values and turbulence levels.

As the meshing for the LES was based on RANS scalings, the resolution in the half opposite to the wall jet is probably insufficient. This shows the limitations of such a priori studies if uncertainties of standard RANS models are not accounted for. The low counter velocity (hence stronger buoyancy) case, BUO1, is probably the most challenging of the three. Gravity waves were observed at the jet separation with the worrying fact that their wavelength was equal to the computational domain width (periodicity conditions are likely to amplify this mode). For completeness, the stronger buoyancy case should be rerun with a wider domain and a finer mesh across the channel. Sensitivity to jet inlet conditions (precursor channel flow LES imposed at inlet) should also be investigated.

Acknowledgements

Y. Addad gratefully acknowledges a Ph.D. grant from the Algerian Ministère de l'Enseignement et de la Recherche Scientifique. The experimental work of He et al. was sponsored by the Industrial Management Committee (British Energy, BNFL Magnox Generation and HSE). For the LES work support from British Energy and BNFL Magnox Generation, and helpful discussions with Dr. M. Rabbitt (British Energy) are also acknowledged.

References

Addad, Y., Laurence, D., Talotte, C., Jacob, M.C., 2003. Large eddy simulation of a forward–backward facing step for acoustic source identification. International Journal of Heat and Fluid Flow 22, 562–571.

Archambeau, F., Mechitoua, N., Sakiz, M. Code Saturne: a finite volume method for the computation of turbulent incompressible flows. International Journal of Finite Volumes (2004).

Baggett, J.S., Jiménez, J., Kravchenko, A.G., 1997. Resolution requirements in large-eddy simulations of shear flows. In: Annual Research Briefs. Center for Turbulence Research, Stanford, pp. 51–66.

Benhamadouche, S., 2001. Modelisation de Sous-Maille pour la LES—Validation sur la Turbulence Homogene Isotrope (THI) dans une Version de Developpement de Code_Saturne, Rapport: HI-83/01/33/A, EDF R&D.

Benhamadouche, S., Laurence, D., 2003. LES, coarse LES, and transient RANS comparisons on the flow across a tube bundle. International Journal of Heat and Fluid Flow 4, 470–479.

Benhamadouche, S., Mahesh, K., Constantinescu, G., 2002. Colocated finite-volume schemes for large-eddy simulation on unstructured meshes. In: Proceedings of the Summer Program, Center for Turbulence Research, NASA Ames/Stanford University. pp.143–154.

Benhamadouche, S., Sakiz, M., Peniguel, C., Stephan, J.M., 2003. Presentation of new methodology of chained computations using instationary 3D approaches in a T-junction of a PWR nuclear plant. In: 17th International Conference on Structural Mechanics in Reactor Technology, August, Prague. pp. 17–22.

Craft, T.J., Gerasimov, A.V., Iacovides, H., Kidger, J.W., Launder, B.E., 2004. The negatively buoyant wall jet: performance of alternative options in RANS modelling. In: Proceedings of 4th International Symposium on Turbulence Heat and Mass Transfer, Antalya, Turkey, 2003, International Journal of Heat and Fluid Flow 25, 809–823.

Ferziger, J.H., Perić, M., 1999. Computational Methods for Fluid Dynamics, second ed. Springer.

Gao, S., Voke, P.R., 1995. Large-eddy simulation of turbulent heat transport in enclosed impinging jets. International Journal of Heat and Fluid Flow 16, 349–356.

He, S., Xu, Z., Jackson, J.D., 2002. An experimental investigation pf buoyancy-opposed wall jet flow. International Journal of Heat and Fluid Flow 23, 487–496.

Jones, W.P., Wille, M., 1996. Large-eddy simulation of plane jet in a cross-flow. International Journal of Heat and Fluid Flow 17, 296–306.

Koutmos, P., Mavridis, C., 1997. A computational investigation of unsteady separated flows. International Journal of Heat and Fluid Flow 18, 297–306.

Mahesh, K., Constantinescu, G., Apte, S., Iaccarino, G., Moin P., 2001. Large eddy simulation of gas turbine combustors. Annual Research Briefs. Center for Turbulence Research, NASA Ames/ Stanford University. pp. 3–19.